IEEE Access
Multidisciplinary | Rapid Review | Open Access Journal

Received March 7, 2020, accepted April 3, 2020, date of publication April 14, 2020, date of current version April 30, 2020.

Digital Object Identifier 10.1109/ACCESS.2020.2987835

A Piecewise Hybrid Stochastic Resonance Method for Early Fault Detection of Roller Bearings

SHAN WANG[1], PINGJUAN NIU[1,2], YONGFENG GUO[3], FUZHONG WANG[4], AND SHUZHEN HAN[1]

[1]School of Mechanical Engineering, Tiangong University, Tianjin 300387, China
[2]School of Electronics and Information Engineering, Tiangong University, Tianjin 300387, China
[3]School of Mathematical Sciences, Tiangong University, Tianjin 300387, China
[4]School of Physical Science and Technology, Tiangong University, Tianjin 300387, China

Corresponding authors: Pingjuan Niu (niupingjuan@tjpu.edu.cn) and Yongfeng Guo (sdjnwsgyf@163.com)

This work was supported in part by the National Natural Science Foundation of China under Grant 11672207, in part by the Tianjin Natural Science Foundation of China under Grant 17JCYBJC15700, and in part by the Program for Innovative Research Team, Tianjin University, under Grant TD13-5035.

ABSTRACT An unsaturated stochastic resonance (USR) method to overcome the output saturation phenomenon observed in the classical bistable stochastic resonance (CBSR) method has been examined. However, the parameters of USR models can lead to inaccurate results while identifying the characteristic frequency amid high levels of background noise. To overcome this limitation, an adaptive piecewise hybrid stochastic resonance (APHSR) method that introduces a parameter μ to improve the performance of fault characteristic detection is proposed. The optimal parameters are determined automatically using both 3D reverse positioning and least-squares methods, combing with signal-to-noise ratio and spectral value as evaluation criteria. The significance of parameter μ is demonstrated by analyzing the critical amplitude and Kramers' escape rate. When the results were evaluated through comparison with the CBSR and USR methods via a simulation and two experiments on a motor and a parallel gearbox, it was demonstrated to be more capable of diagnosing the early faults of rotating machinery especially in high levels of background noise.

INDEX TERMS Early fault detection, weak characteristic extraction, piecewise hybrid stochastic resonance.

I. INTRODUCTION

The early detection of bearing faults can help to ensure the safety and reliability of machinery [1]. However, early detection is not straightforward as the impulse energy caused by a fault only represents a small proportion of the total vibration energy of a bearing system and is distributed across a wide frequency range. Moreover, these vibrations are typically masked by a large amount of environmental interference in the form of noise and the other vibrations produced by adjacent mechanical components and systems [2], thereby making early fault detection more difficult. To overcome this challenge, various weak signal detection approaches have been introduced to extract the features of faults from the noise, such as wavelet decomposition [3], [4], singular value decomposition [5], fractional-order entropy infograms [6], spectral kurtosis [7], [8], the local outlier factor [9], and time-frequency analysis algorithms [10], [11], and machine learning [12]–[14], all of which are designed to remove noise from signals so that the fault characteristics can be recognized. An alternative approach is to recognize the noise as a type of signal energy that can be assist in the extraction of periodic signal features. This approach is adopted in the noise-assisted data processing method known as the stochastic resonance (SR) method. Unlike conventional denoising techniques, the SR method can be used to detect weak signals by utilizing noise to enhance the features of weak signals.

The term SR was first coined by Benzi *et al.* and has been used to explain variations in the Earth's climate between the ice ages and periods of relative warmth over a roughly 100,000 year cycle [15]–[17]. Fauve and Heslot [18] and McNamara *et al.* [19] observed the SR phenomenon in Schmitt-trigger circuits and in a bidirectional ring laser, respectively, thereby confirming the validity of the SR approach. Several studies have investigated the conditions under which SR is observed or the signal-to-noise ratio (SNR) is maximized. Tan *et al.* [20] proposed a frequency-shifted and re-scaled SR method to reduce the influence of a high

The associate editor coordinating the review of this manuscript and approving it for publication was Mohamed Elhoseny.

sampling frequency and a large number of sample points. Chapeau-Blondeau *et al.* presented a generic dynamic model with saturation for neural signal transduction at the synaptic stage [21]. He and Wang [22] explored a new mechanism of SR that is induced by noise at multiple scales to enhance the detection of weak signals under heavy background noise. It should be noted that these studies only investigated saturated SR. Zhao *et al.* [23] demonstrated that unsaturated stochastic resonance (USR) overcome the limitation of output saturation of classical bistable stochastic resonance (CBSR) while extracting weak signal characteristics. Qiao *et al.* [24] discovered that USR system without output saturation can improve the output SNR. Wang and Xia [25] demonstrated that output saturation produces a local optimal output signal. Guo *et al.* [26] investigated the steady-state properties of a piecewise nonlinear bistable model driven by multiplicative and additive Gaussian colored noise with colored cross correlation. Although these studies focused on reducing the influence of output saturation in the CBSR approach, it is desirable to improve the performance of this method while avoiding the saturation phenomenon during the extraction of the characteristics of weak faults amid high levels of background noise.

In this study, a novel adaptive piecewise hybrid stochastic resonance (APHSR) method is proposed to improve the performance of weak signal detection in the fault diagnosis of rolling bearings. Specifically, the method is designed to realize the adaptive extraction of periodic signal features even when they are buried under high levels of noise. In this method, the parameter μ leverages the critical amplitude (A_c) and Kramers' escape rate, both of which contribute to the high processing ability of the SR method, and the optimal model parameters are obtained automatically using the 3D reverse positioning and least-squares methods with the SNR and spectral value (SV) as evaluation criteria. The results of the simulations and experiments presented in this paper demonstrate that the proposed APHSR method can effectively extract periodic features for bearing fault diagnosis.

A. CONTRIBUTIONS

The key contributions of this work are as follows.

1) An APHSR method with the introduction of the parameter μ is proposed to extract weak fault characteristics from early defects of roller bearings.
2) 3D reverse positioning and least-squares methods are established and the SNR and SV are defined as evaluation criteria to obtain the optimal parameters.
3) The proposed APHSR method is demonstrated by using two experiments including a motor and parallel gearboxes in which it outperforms the CBSR and USR methods.

B. OUTLINE

The remainder of this paper is structured as follows. The CBSR and USR models are briefly introduced in Section 2. The APHSR model for extracting incipient fault characteristics is described in Section 3. A simulation of the APHSR method when used in the fault diagnosis of a rolling bearing is provided in Section 4. The proposed method was validated using experiments on a motor bearing and a parallel gear bearing, the results of which are detailed in Section 5. Finally, the conclusions drawn from this study are discussed in Section 6.

II. THEORETICAL BACKGROUND

In the CBSR system, a particle is driven by both periodic and random forces, and a moderate amount of noise can be used to supplement the periodic motion, which is described by the Langevin equation expressed as [27]–[29]:

$$\mathrm{d}x/\mathrm{d}t = -\mathrm{d}U_{\mathrm{o}}(x)/\mathrm{d}x + \mathrm{s}(t) + \xi(t) \tag{1}$$

where the weak periodic signal $s(t) = A\cos(2\pi f_0 t + \varphi)$, f_0 is the characteristic frequency, A is the amplitude of the periodic signal, φ is the corresponding phase, x is the output signal of the classical bistable system, $\xi(t)$ is the zero mean Gaussian white noise, $E[\xi(t)\xi(t+\tau)] = 2D\delta[t-\tau]$, and D is the noise intensity. If there is no input signal, i.e. when $A = 0$V and $D = 0$V, the potential function can be written as follows [30]:

$$U_o(x) = -\frac{a}{2}x^2 + \frac{b}{4}x^4 \tag{2}$$

where a and b are non-zero theoretical parameters.

To illustrate the saturation characteristics of CBSR, a numerical simulation was conducted using the following conditions: the input signal was $s(t) = A\cos(2\pi ft)$, the theoretical parameters were $a = b = 1$, the signal frequency was $f = 0.01$ Hz, the sampling frequency was $fs = 10$ Hz, and the A values were 0.4, 0.8, 1.2, 1.6, and 2.0 V. The model was initially applied in a no-noise state, i.e., $D = 0$ V. As shown in Fig. 1(a), when the amplitude $A = 0.4$ V, there was no transition between the bistable states and the particles only moved in one potential well. Subsequently, as A increased, the output amplitude did not vary significantly and exhibited a stable value of approximately 1.5 V, which indicated saturation. As shown in Fig. 1(d), under heavy background noise, i.e. $D = 20$ V, only a rough outline of the output of the bistable model can be seen along with distinct saturation behavior.

To overcome the inherent output saturation of the CBSR and improve the performance of signal detection, the USR theory was introduced by Zhao *et al.* [23]. It can be expressed as follows:

$$U(x) = \begin{cases} -\dfrac{a^2}{4b}\left(\dfrac{x+c}{c-\sqrt{a/b}}\right), & x < -\sqrt{a/b} \\ -\dfrac{a}{2}x^2 + \dfrac{b}{4}x^4, & -\sqrt{a/b} \le x \le \sqrt{a/b} \\ \dfrac{a^2}{4b}\left(\dfrac{x-c}{c-\sqrt{a/b}}\right), & x > \sqrt{a/b} \end{cases} \tag{3}$$

where a and b are positive real values, and $c = \sqrt{2a/b}$.

The same simulation was conducted to illustrate the unsaturated characteristics of the USR and its shortcomings under

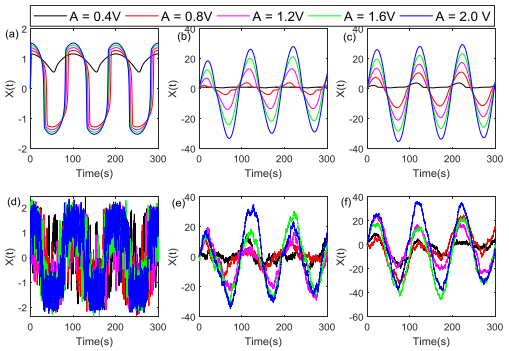

FIGURE 1. Outputs of the different methods with varied amplitudes and noise intensities: (a) CBSR theory with $D = 0$ V, (b) USR theory with $D = 0$ V, (c) APHSR theory with $D = 0$ V, (d) CBSR theory with $D = 20$ V, (e) USR theory with $D = 20$ V, and (f) APHSR theory with $D = 20$ V.

heavy background noise. The parameters were as follows: $a = b = 1$ and $c = \sqrt{2}$. Fig. 1(b) shows the output time-domain diagrams of the model with no noise. Unlike the CBSR model, the output amplitude of the USR model increases with the increasing signal amplitude, and there is no output saturation phenomenon. As shown in Fig. 1(e), when the noise intensity $D = 20$ V, although the outline can be recognized, it is blurred by the noise, which may lead to an inaccurate bearing fault diagnosis.

III. PROPOSED APHSR THEORY

The USR method has been applied to rotating machinery fault diagnosis for years and has achieved good results. In the early stage of bearing faults, however, using USR theory to detect the signals is difficult since potential periodic impulses are often overwhelmed by unexpected heavy noise. Therefore, the proposed APHSR theory introduces the parameter μ to improve the performance of bearing fault diagnosis.

A. PIECEWISE HYBRID POTENTIAL BISTABLE MODELS

The potential function is as follows:

$$\mathrm{U}(x) = \begin{cases} -\dfrac{\sqrt{\mathrm{a}^3/b}}{4\,(\mu-1)}(x+\mu\sqrt{a/b}), & x < -\sqrt{a/b} \\ -\dfrac{\mathrm{a}}{2}x^2 + \dfrac{b}{4}x^4, & \sqrt{a/b} \le x \le -\sqrt{a/b} \\ \dfrac{\sqrt{\mathrm{a}^3/b}}{4\,(\mu-1)}(x-\mu\sqrt{a/b}), & x > \sqrt{a/b} \end{cases} \tag{4}$$

where $a > 0$, $b > 0$, $\mu > 1$. The critical amplitude and Kramers' escape rate are used as evaluation criteria to clarify the importance of μ. In Eq. (4), when the periodic signal $s(t)$ exists and the noise signal $n(t) = 0$, the theoretical potential function is periodically modulated by the characteristic signal from $U(x)$ to $V(x)$:

$$V(x) = U(x) - xA\cos(2\pi f_0 t + \varphi) \tag{5}$$

As shown in Fig. 2, the two potential wells of the potential function are periodically raised or deepened. Moreover, there is a critical amplitude, which maintains the bistable structure.

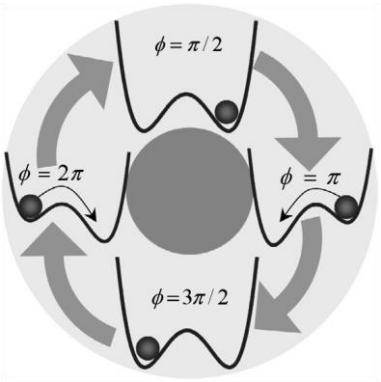

FIGURE 2. Periodic variation of the potential function of CBSR theory due to modulation by a periodic signal.

At this critical amplitude, the modulated potential function $V(x)$ changes from a bistable structure to a monostable structure when $A\cos(2\pi f_0 t + \varphi)$ is at its maximum or minimum value. This means that the position of a potential well changes from a pole to an inflection point. Therefore, the generation of stochastic resonance requires a smaller critical amplitude. Taking the maximum value of $A\cos(2\pi f_0 t)$ at the time $t = -\varphi/(2\pi f_0)$ as an example, $V(x)$ needs to satisfy the following relationship [31]:

$$\begin{cases} \dfrac{\mathrm{d}U(x)}{dx} = -ax + bx^3 - A = 0 \\ \dfrac{\mathrm{d}^2U(x)}{\mathrm{d}x^2} = -a + 3bx^2 = 0 \end{cases} \tag{6}$$

The critical amplitude of the CBSR theory is obtained through Eq. (7).

$$Ac_0 = \sqrt{\frac{4a^3}{27b}} \tag{7}$$

Similarly, the critical amplitude of the APHSR theory should be satisfied:

$$\mathrm{Ac} = \begin{cases} \dfrac{\sqrt{a^3/b}}{4(\mu-1)}, & x < -\sqrt{a/b} \\ \sqrt{\dfrac{4a^3}{27b}}, & -\sqrt{a/b} \le x \le \sqrt{a/b} \\ \dfrac{\sqrt{a^3/b}}{4(\mu-1)}, & x > \sqrt{a/b} \end{cases} \tag{8}$$

As depicted in Fig. 3(a) where $a = 0.5\sim2$, $b = 1$ and $\mu = \sqrt{1.5}, \sqrt{2.0}, \sqrt{3.0}$, the $\mathrm{A_c}$ of the APHSR method decreases as μ increases. It is noted that the $\mathrm{A_c}$ is lower than the CBSR and USR methods only in case of the optimal parameter μ. With the same parameters a and b, the value of $\mathrm{A_c}$ is calculated using Eq. (8) and it is lower than CBSR method when $\mu < 1 + 3\sqrt{3}/8$ and lower than USR method when $\mu > \sqrt{2}$. The results of analysis demonstrate the importance of parameter μ to the critical amplitude and further influence the effectiveness of stochastic resonance system.

To further validate the usefulness of the μ parameter, the Kramers' escape rate of the APHSR method was deduced

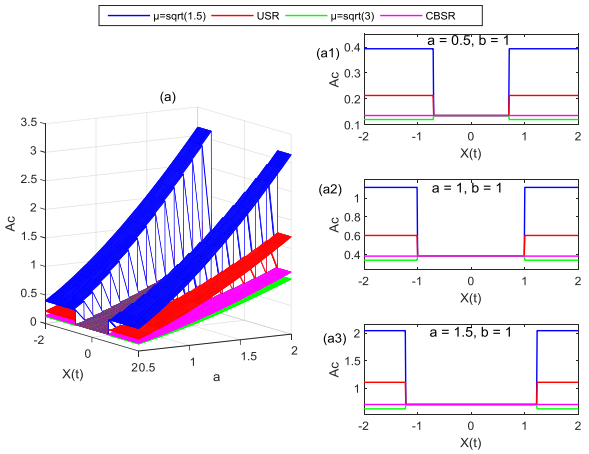

FIGURE 3. Critical amplitudes and outputs of the CBSR, USR, and APHSR theories with different μ parameters.

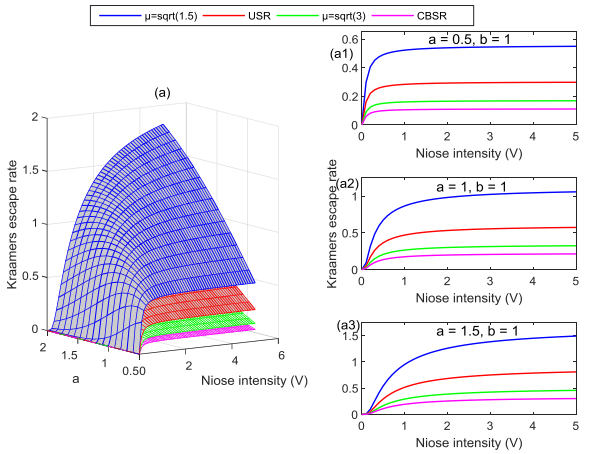

FIGURE 4. Kramers' escape rate obtained through the CBSR, USR, and APHSR theories with different μ parameters.

via adiabatic approximation. The Kramer's escape rate as per the CBSR method can be expressed as follows [32]:

$$r_k = \frac{a}{\sqrt{2}\pi} \exp(-\frac{a^2}{4bD}) \tag{9}$$

The potential function of the CBSR method as per Eq. (2) can be replaced with the potential function of the APHSR method shown in Eq. (4). According to the adiabatic approximation, the mean first passage time $\tau_{\pm}$ of the process $x(t)$ to reach the state $x_{\pm}$ is given by Kramers' time:

$$\mathrm{r}_{-}^{-1}(t) = \frac{1}{D}\left[\int_{-\mu\sqrt{a/b}}^{-\sqrt{a/b}} \exp\left[-\frac{\sqrt{a^3/b}}{4D}(\frac{x+\mu\sqrt{a/b}}{1-\mu})\right]dx\right] \times \left[\int_{-\sqrt{a/b}}^{0} \exp\left[\frac{1}{D}(-\frac{a}{2}x^2+\frac{b}{4}x^4)\right]dx\right] \tag{10}$$

When $A \ll 1, \mathrm{D} \ll 1$, the final results can be obtained as follows:

$$\mathrm{r}_{-}^{-1}(t) \approx \frac{4(\mu-1)}{\mathrm{a}} \exp(\frac{a^2}{4bD}) \tag{11}$$

Similarly,

$$\mathrm{r}_{+}^{-1}(t) = \frac{1}{D}\left[\int_{0}^{\sqrt{a/b}} \exp\left[\frac{1}{D}(-\frac{a}{2}x^2+\frac{b}{4}x^4)\right]dx\right] \times \left[\int_{\sqrt{a/b}}^{\mu\sqrt{a/b}} \exp\left[\frac{\sqrt{a^3/b}}{4D}(\frac{x+\mu\sqrt{a/b}}{1-\mu})\right]dx\right] \approx \frac{4(\mu-1)}{\mathrm{a}} \exp(\frac{a^2}{4bD}) \tag{12}$$

Therefore, the Kramers' escape rate of the APHSR method is as follows:

$$r_k = \frac{a}{4(\mu-1)} \exp(-\frac{a^2}{4bD}) \tag{13}$$

To compare the CBSR, USR and APHSR methods, the distribution of Kramers' escape rates is shown in Fig. 4, where $a = 0.5{\sim}2$, $b = 1$ and $\mu = \sqrt{1.5}, \sqrt{2.0}, \sqrt{3.0}$. It is apparent that the Kramers' escape rate of the APHSR method decreases as μ increases and is higher than the CBSR and USR methods only when the value of μ is optimal. According to Eq. (13), the APHSR Kramers' escape rate value is higher than the CBSR method when $\mu < 1 + \sqrt{2}\pi/4$ and is higher than USR method when $\mu < \sqrt{2}$. The data indicate that parameter μ influences the Kramers' escape rate and contributes to SR generation.

Similar simulations were used to analyze the APHSR method proposed in this study using parameters $a = b = 1$ and $\mu = 2$. The output time-domain diagrams of the proposed model are shown in Fig. 1(c) and (f). It should be noted that the output of the APHSR method is both larger and less noisy than those of the CBSR and USR methods, thereby indicating that the proposed method is more robust and better able to detect weak signals amid high levels of noise.

B. APHSR SYSTEM FOR WEAK BEARING FAULT DETECTION

In the proposed APHSR method, the SNR and SV are used as evaluation criteria [33] to determine the optimal parameters via the least-squares and 3D reverse positioning methods. A flowchart of the approach is shown in Fig. 5, where a, b and μ are the parameters for the cycles of n1, n2, and n3, respectively. The SNR is computed as $\mathrm{SNR} = 10\log\left(\mathrm{p}_s/p_n\right)$ in the form of a matrix (n1, n2, n3), where p_s and p_n represent the effective powers of the signal and noise, respectively. When the values of a, b and μ have been selected, the output SNR of the model is computed and stored in the matrix. Then, the maximum SNR is calculated and stored before its corresponding SV is calculated and stored in a column vector. Finally, the maximum SV ($\mathrm{SV}_{\max}$) of the model is calculated. Using the value of $\mathrm{SV}_{\max}$, the optimal parameters a, b and μ can be determined automatically using the 3D reverse positioning method [34].

A diagram of the proposed APHSR method for extracting weak fault characteristics from a noisy signal is shown in Fig. 6. It should be noted that the output signal can be optimized by tuning the parameters.

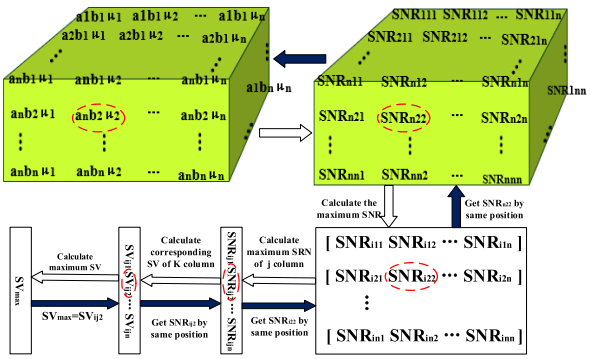

FIGURE 5. Flowchart of the APHSR method.

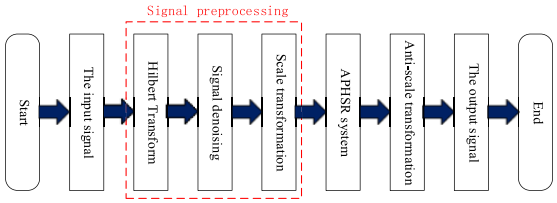

FIGURE 6. Proposed APHSR system for mechanical fault diagnosis.

To quantitatively evaluate the influence of parameter selection, the SNR was calculated for the envelope spectrum of repetitive transients. The SNR is defined as follows [35]:

$$SNR = 10\log_{10}\left(\frac{A_d}{\sum_{i=1}^{N/2} A_i - A_d}\right) \tag{14}$$

Here, i (0, 1 . . . N) denotes the order of the harmonic, A_i represents the amplitude of the i^{th} extracted harmonic, and the denominator $\sum_{i=1}^{N/2} A_i - A_d$ represents the power amplitude sum of the noise in the output power spectrum. A higher SNR implies that the amplitude of the fault characteristic frequency and its harmonics are more dominant in the envelope spectrum, indicating a fault in the rotating machinery. The process of detecting a weak fault signal using the APHSR theory is as follows:

(1) Signal preprocessing: First, the envelope signal is obtained via Hilbert transform demodulation. Because the original signal is extremely noisy, the empirical mode decomposition denoising method is used to remove the high-frequency noise [36], [37], and a Chebyshev filter is applied to remove any low-frequency noise from the signal [38]. Then, the remaining components are reconstructed to obtain a filtered signal.

(2) Optimizing the theoretical parameters: The optimization ranges of parameters a, b, and μ are set as (0, 20], (0, 20], and (1, 3], respectively. The optimal parameters are then computed using the two evaluation criteria (SNR and SV) and the least-squares and 3D reverse positioning methods.

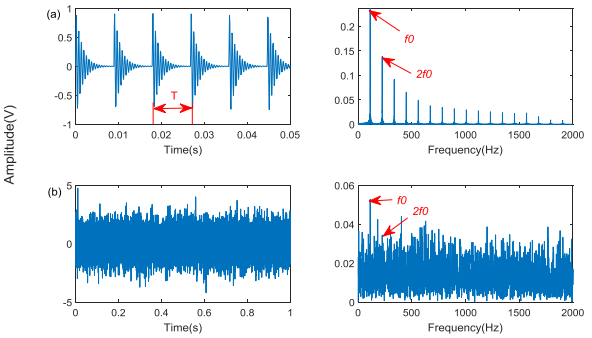

FIGURE 7. Simulated signals: (a) repetitive transients, and (b) noised signal.

(3) Weak fault feature detection: In this step, the optimal parameters are input into the APHSR model, the scale is recovered, and the output signal is obtained. Then, the weak fault features are separated from the noisy background in the output signal. Finally, the results are analyzed to detect the presence of faults in the bearing of interest.

IV. SIMULATION

The following simulation model was used to generate a series of transient signals [39], [40]:

$$\chi_n(t) = B(t)\sum_q \chi(t - q/f_0) + N(t) \tag{15}$$

Here, $B(t)$ represents the amplitude of the repetitive transients ($B(t) = 0.7$), q is the number of transients, f_0 denotes the fault characteristic frequency ($f_0 = 112$ Hz), $N(t)$ represents the random noise, and $\chi(t)$ represents the periodic impulse response function given by

$$\chi(t) = \begin{cases} \exp(-\beta_w t)\sin(2\pi f_{re} t), & t > 0 \\ 0, & t \le 0 \end{cases} \tag{16}$$

Here, β_w represents the structural damping ratio ($\beta_w = 666.67$), and f_{re} represents the resonance frequency ($f_{re} = 1683.40$ Hz). In this simulated case, f_s is the sampling frequency with a value of 12 kHz, and the sampling time is 1 s.

To simulate a bearing fault signal under a heavy noise background, Gaussian white noise with a noise intensity $D = 1$ V was added to the pure repetitive transients, and a noisy signal $\chi_n(t)$ was then obtained. The simulated bearing fault signal is displayed in Fig. 7(a) with an impulse interval of approximately 0.009 s. It is evident that the impulse components are completely buried in the noise as shown in Fig. 7(b), which mimics the real working environment of the machinery. In the envelope spectrum, the weak fault characteristic frequency and its second harmonic cannot be clearly observed.

To verify the effectiveness of the proposed method, the envelope signal was preprocessed, and the following parameter values were automatically obtained using the adaptive algorithm, giving $a = 4$, $b = 3.2$, and $\mu = 1.05$. The time-domain waveform and envelope spectrum of the

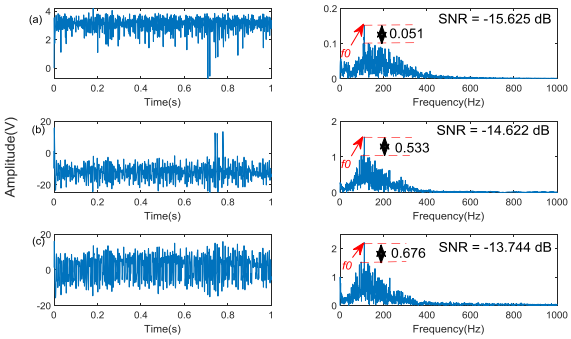

FIGURE 8. Output signals and their envelope spectra using different methods: (a) CBSR theory, (b) USR theory, and (c) APHSR theory.

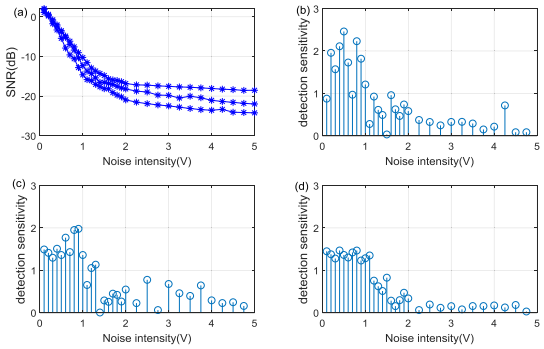

FIGURE 9. (a) Output SNR of the three methods with different noise intensities; the detection sensitivity of (b) CBSR theory, (c) USR theory, and (d) APHSR theory.

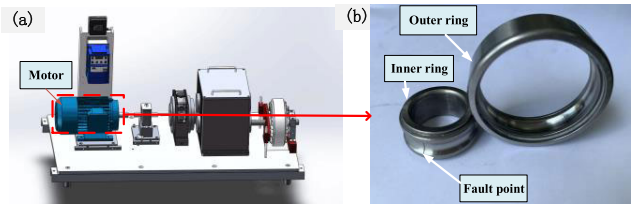

FIGURE 10. (a) Experimental drivetrain diagnostics simulator (DDS) equipment, and (b) motor bearing fault.

simulation signal were obtained by substituting the optimal parameters into the APHSR model, as shown in Fig. 8(c). The characteristic frequencies are clearly visible. The SNR of the proposed model is −13.744 dB, and the maximum amplitude is 0.676 V [41] higher than the ambient noise, thus verifying the effectiveness of the model.

To demonstrate the superiority of the proposed method, the simulation signal was also processed using the CBSR and USR models so that the results could be compared. The optimal parameters of the CBSR and USR models computed using the adaptive algorithm were ($a = 0.2$, $b = 0.02$) and ($a = 3.4$, $b = 1.6$), respectively. The time-domain and envelop spectrum diagrams of the CBSR and USR models are shown in Fig. 8(a) and (b), respectively. Although the characteristic frequencies are visible, their recognizable degrees are only 0.051 and 0.533 V. When these results were compared to those of the proposed method, the spectral peaks of the characteristic frequencies were more distinct in the latter with recognizable degree gains of 0.626 and 0.143 V and SNR gains of 1.881 and 0.878 dB, respectively. Based on these results, the proposed APHSR method effectively overcame the saturation characteristics in the presence of high levels of noise. The new variable μ provided a useful means to optimize the parameters, which increased the effectiveness and practicality of the proposed method compared to the alternatives.

To verify the applicability of the proposed method, the noise intensity was set in the range of 0.1∼5 V, the second sampling frequency fs_2 was set to 2 Hz, and the originally acquired signals were provided as inputs to the CBSR, USR, and APHSR models. As shown in Fig. 9, the output SNR and detection sensitivity ratio of the models varied with the noise intensity [42].

As shown in Fig. 9(a), the output SNR decreased as the input noise intensity increased and the output SNR of the proposed method was higher than those of the other two methods. The highest SNR gains were 5.7 and 3.46 dB, respectively, at $D = 5$ V. As shown in Fig. 9(b), (c), and (d), the SNR curve of the proposed method was smooth, and the detection sensitivity was less than 1.5. The detection sensitivity of the proposed method was lower than those of the CBSR and USR methods by a maximum of 66% and 33%, respectively. This indicates that the APHSR model is more efficient at extracting the bearing fault characteristic frequency signals in the presence of high levels of background noise.

V. EXPERIMENTAL DEMONSTRATION

As bearings are widely used in modern machinery, any faults that arise in them may lead to the fatal breakdown of a machine. To reduce the risk of catastrophic machine failure, fault diagnoses are conducted on bearings to reduce breakdown loss and ensure personnel safety. In this section, the results of two experiments conducted on a real motor rolling bearing and a parallel gearbox rolling bearing are described to demonstrate the effectiveness of the proposed method.

A. MOTOR BEARING EXPERIMENT

A pitting fault on the inner ring of a motor bearing was taken as an example to verify the effectiveness of the proposed method. The test device was based on a real motor bearing with a slight flaking fault on the inner race, as shown in Fig. 10.

The sampling frequency was set as $f_s = 12.8$ kHz, the number of sampling points was 16384, and the rotational speed was 15 rev/min. Table 1 lists the parameters of the rotor bearing. Combined with the vibration theory analysis, the fault frequency of the inner ring (f_{inner}) of the motor bearing was calculated to be 73.98 Hz.

A time-domain waveform and envelope spectrum of the inner ring fault of the bearing is shown in Fig. 11, where the influence of noise on the signal is evident. Although

TABLE 1. Rotor bearing parameters.

Component	Mfg.	Brg.No.	# of R. E.	BPFO	BPFI
Motor bearing	NSK	6203	8	3.066	4.932

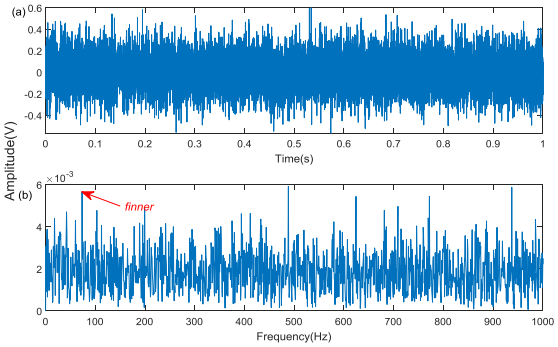

FIGURE 11. Input signal of (a) the time-domain waveform, and (b) the envelope spectrum.

the characteristic frequency of 73.24 Hz is visible in the spectrum, there is also a large amount of noise across the frequency band, which makes it difficult to identify the faults.

B. PARALLEL GEARBOX BEARING EXPERIMENT

In the second experiment, a vibration signal from a parallel gearbox bearing was analyzed to further demonstrate the effectiveness of the APHSR method. In this experiment, a pitting fault in the secondary parallel gearbox bearing of a gearbox diagnostics simulator (GDS) was studied. Physical drawings and a schematic of the gearbox are shown in Fig. 13(a). The first and second gears constitute the first gear train, while the third and fourth gears constitute the second gear train. The faulty bearing is located in the end cover near the third gear and the specific point of the fault is shown in Fig. 13(b).

In this experiment, $f_s = 51.2$ kHz, the number of sampling points was 65,536, and the rotational speed of the primary bearing was 40 rev/min. The parameters of the gear trains are listed in Table 2. After the deceleration of the first gear train, the speed of the second gear train decreased, resulting in a bearing speed of 11.6 rev/min. Using vibration analysis, the characteristic frequency of the fault in the secondary bearing outer ring (f_{outer}) of the parallel gearbox was found to be 41.04 Hz.

The fault features were extracted using the proposed method. After preprocessing, the following parameter values

TABLE 2. Parallel gearbox parameters.

	Primary gear train		Secondary gear train	
Tooth number	Input	Output	Input	Output
	29	100	36	90
Speed (rev/min)	40		11.6	

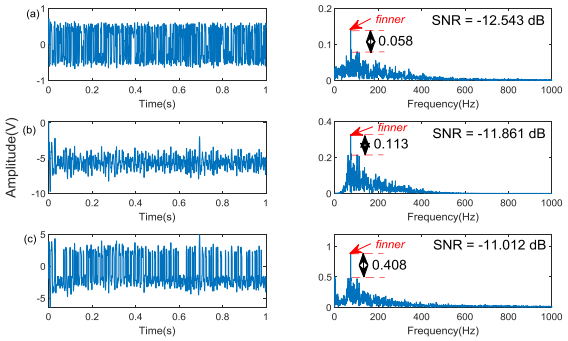

FIGURE 12. Time-domain waveform and envelope spectrum of the output signal for (a) CBSR theory, (b) USR theory, and (c) APHSR theory.

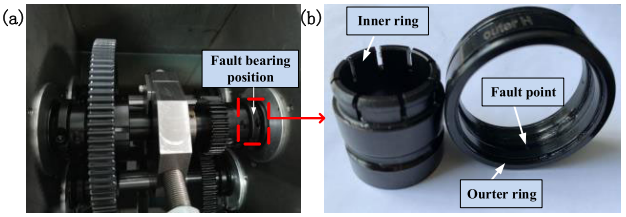

FIGURE 13. (a) Physical drawing of gearbox, and (b) fault bearing.

were obtained: $a = 3.2$, $b = 1.8$, and $\mu = 1.2$. The parameters were input to the APHSR model to obtain the time-domain waveform and envelope spectrum of the inner ring fault signal, as shown in Fig. 12(c). The spectral peak of the characteristic frequency is visible in the figure and is 0.408 V higher than the ambient noise amplitude and the output SNR is -11.012 dB. To compare the diagnostic effect of the proposed method with the CBSR and USR methods in engineering applications, the fault signals were processed using these two methods, which resulted in the following parameter values: ($a = 0.1$, $b = 0.6$) and ($a = 7$, $b = 2.6$), respectively. The time-domain waveform and envelope spectrum are shown in Fig. 12(a) and (b), respectively. Owing to the saturation of the CBSR output and the inadequacy of the USR parameters, the recognizable degrees of the characteristic frequencies amplitudes of the CBSR and USR methods were only 0.058 and 0.113 V, which are 6 and 2.6 times lower than the APHSR method; the output SNRs of the CBSR and USR methods were only -12.543 and -11.861 dB, which are 1.531 and 0.849 dB lower than the APHSR method. These data indicate that the proposed method provides a higher amplitude recognizable degree and a higher SNR, and is better able to identify the fault signal than the CBSR and USR methods.

To acquire the characteristic frequency of the fault, the collected signals were processed to obtain the time-domain waveform and envelope spectrum shown in Fig. 14. Note that it is not possible to determine the characteristic frequency of the fault from either the time-domain waveform or the envelope spectrum due to the high levels of noise. Therefore, the collected signals were processed via the CBSR, USR, and APHSR methods. As per the APHSR method, the optimal parameter values were computed to be $a = 5.2$, $b = 2.4$,

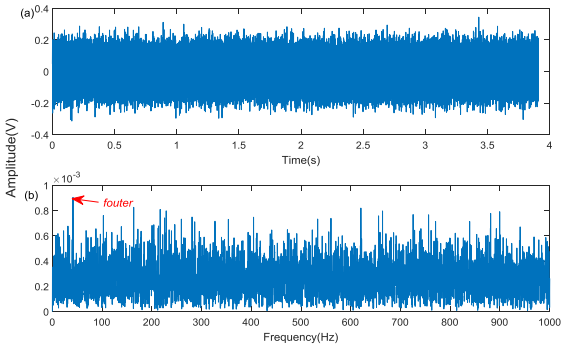

FIGURE 14. (a) Time-domain waveform, and (b) envelop spectrum of input signal.

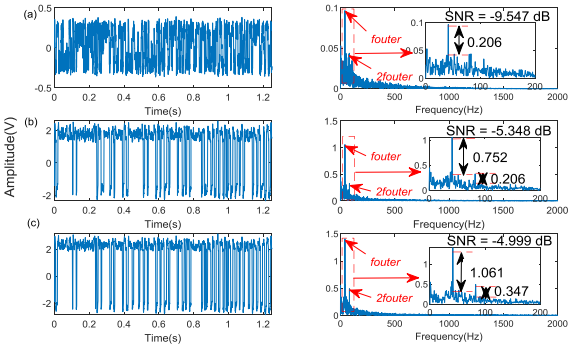

FIGURE 15. Time-domain waveform and envelope spectrum of the output signal with (a) CBSR theory, (b) USR theory, and (c) APHSR theory.

and $\mu = 1.3$. The time-domain waveform and envelope spectrum were obtained by inputting the parameters into the model and are shown in Fig. 15(c), where the characteristic frequency (41.41 Hz) is visible. Based on the values listed in Table 2, this value is consistent with the theoretical value (41.04 Hz) of the signal coming from the outer ring bearing of the secondary gearbox, which indicates that the fault on the outer ring of the secondary bearing was correctly identified, thereby verifying the effectiveness of the proposed method.

The parameters of the CBSR and USR models were determined to be ($a = 0.05$, $b = 0.75$) and ($a = 8$, $b = 2.4$), respectively. The time-domain waveform and envelope spectrum of the CBSR and USR methods are shown in Fig. 15(a) and (b). In Fig. 15(a), while the characteristic frequency can be seen, the double-frequency was distorted by the noise caused by the saturation characteristics, vibration complexity, and the influence of sensor noise in the signal acquisition process. Although the USR method provided the characteristic frequency and the corresponding double frequency, as shown in Fig. 15(b), their amplitudes were only 0.752 and 0.206 V higher than the surrounding noise, and the SNR was only -5.348 dB. Compared with the proposed method, the recognizable degree of the characteristic and double-frequencies decreased by 41% and 68%, respectively, and the output SNR decreased by 6.5%. The data demonstrates that the proposed method is effective when extracting complex signals from noise.

These results confirm that the APHSR method is capable of detecting weak fault characteristics buried in high levels of noise and that the performance of the proposed method is higher than the CBSR and USR methods when identifying early faults in bearings.

VI. CONCLUSION

In this paper, an APHSR method was proposed to improve the performance of fault detection using vibration signals distorted by high levels of noise. The following conclusions were drawn from this work based on the results of the theoretical and experimental investigations conducted in this study:

1) The introduction of parameter μ has a positive effect on the APHSR. The proposed method included a parameter denoted by μ, the influence of which on the critical amplitude and Kramers' escape rate is analyzed and further of the APHSR to improve fault detection performance.
2) The APHSR method is capable of identifying bearing fault characteristics in the presence of high levels of background noise. In the method, the SNR and SV were selected as evaluation criteria with which the optimal parameters were obtained automatically via the 3D reverse positioning and least-squares methods. The method was validated using simulations and experiments including a motor bearing and a gearbox bearing. The results demonstrate that the proposed method is more capability on suppressing the background noise and extracting the weak fault characteristics from the vibration signals when than the CBSR and USR methods.
3) As the CBSR method is sensitive to low-frequency components and easily affected by interference from low-frequency noise, in the future, further research will be conducted into the preprocessing of low-frequency signals in the form of a theoretical analysis.

ACKNOWLEDGMENT

The authors would like to thank Dr. Zijian Qiao from Ningbo University for valuable suggestions and discussions.

REFERENCES

[1] Z. Qiao, Y. Lei, and N. Li, "Applications of stochastic resonance to machinery fault detection: A review and tutorial," *Mech. Syst. Signal Process.*, vol. 122, pp. 502–536, May 2019.
[2] P. Shi, D. Yuan, D. Han, Y. Zhang, and R. Fu, "Stochastic resonance in a time-delayed feedback tristable system and its application in fault diagnosis," *J. Sound Vibrat.*, vol. 424, pp. 1–14, Jun. 2018.
[3] Z. K. Peng and F. L. Chu, "Application of the wavelet transform in machine condition monitoring and fault diagnostics: A review with bibliography," *Mech. Syst. Signal Process.*, vol. 18, no. 2, pp. 199–221, Mar. 2004.
[4] S. Prabhakar, A. R. Mohanty, and A. S. Sekhar, "Application of discrete wavelet transform for detection of ball bearing race faults," *Tribol. Int.*, vol. 35, no. 12, pp. 793–800, Dec. 2002.
[5] M. Kang and J.-M. Kim, "Singular value decomposition based feature extraction approaches for classifying faults of induction motors," *Mech. Syst. Signal Process.*, vol. 41, nos. 1–2, pp. 348–356, Dec. 2013.
[6] M. Costa, A. L. Goldberger, and C.-K. Peng, "Multiscale entropy analysis of complex physiologic time series," *Phys. Rev. Lett.*, vol. 89, no. 6, Jul. 2002, Art. no. 068102.

[7] Y. Wang, J. Xiang, R. Markert, and M. Liang, "Spectral kurtosis for fault detection, diagnosis and prognostics of rotating machines: A review with applications," *Mech. Syst. Signal Process.*, vols. 66–67, pp. 679–698, Jan. 2016.
[8] T. Barszcz and R. B. Randall, "Application of spectral kurtosis for detection of a tooth crack in the planetary gear of a wind turbine," *Mech. Syst. Signal Process.*, vol. 23, no. 4, pp. 1352–1365, May 2009.
[9] Z. Qiao, Y. Lei, J. Lin, and S. Niu, "Stochastic resonance subject to multiplicative and additive noise: The influence of potential asymmetries," *Phys. Rev. E, Stat. Phys. Plasmas Fluids Relat. Interdiscip. Top.*, vol. 94, no. 5, Nov. 2016, Art. no. 052214.
[10] K. Yu, H. Ma, H. Han, J. Zeng, H. Li, X. Li, Z. Xu, and B. Wen, "Second order multi-synchrosqueezing transform for rub-impact detection of rotor systems," *Mechanism Mach. Theory*, vol. 140, pp. 321–349, Oct. 2019.
[11] L. Li, H. Cai, Q. Jiang, and H. Ji, "An empirical signal separation algorithm for multicomponent signals based on linear time-frequency analysis," *Mech. Syst. Signal Process.*, vol. 121, pp. 791–809, Apr. 2019.
[12] F.-P. An, "Rolling bearing fault diagnosis algorithm based on FMCNN-sparse representation," *IEEE Access*, vol. 7, pp. 102249–102263, 2019.
[13] Q. Jiang, F. Chang, and B. Sheng, "Bearing fault classification based on convolutional neural network in noise environment," *IEEE Access*, vol. 7, pp. 69795–69807, 2019.
[14] M. Elhoseny and K. Shankar, "Reliable data transmission model for mobile ad hoc network using signcryption technique," *IEEE Trans. Rel.*, early access, Jun. 6, 2019, doi:10.1109/TR.2019.2915800.
[15] R. Benzi, A. Sutera, and A. Vulpiani, "The mechanism of stochastic resonance," *J. Phys. A, Math. Gen.*, vol. 14, pp. 453–457, Nov. 1981.
[16] S. Lu, Q. He, and F. Kong, "Effects of underdamped step-varying second-order stochastic resonance for weak signal detection," *Digit. Signal Process.*, vol. 36, pp. 93–103, Jan. 2015.
[17] L. Xu, F. Duan, D. Abbott, and M. D. McDonnell, "Optimal weighted suprathreshold stochastic resonance with multigroup saturating sensors," *Phys. A, Stat. Mech. Appl.*, vol. 457, pp. 348–355, Sep. 2016.
[18] S. Fauve and F. Heslot, "Stochastic resonance in a bistable theory," *Phys. Lett. A*, vol. 97, pp. 5–7, 1983.
[19] B. McNamara, K. Wiesenfeld, and R. Roy, "Observation of stochastic resonance in a ring laser," *Phys. Rev. Lett.*, vol. 60, no. 25, pp. 2626–2629, Jun. 1988.
[20] J. Tan, X. Chen, J. Wang, H. Chen, H. Cao, Y. Zi, and Z. He, "Study of frequency-shifted and re-scaling stochastic resonance and its application to fault diagnosis," *Mech. Syst. Signal Process.*, vol. 23, no. 3, pp. 811–822, Apr. 2009.
[21] F. Chapeau-Blondeau, F. Duan, and D. Abbott, "Synaptic signal transduction aided by noise in a dynamical saturating model," *Phys. Rev. E, Stat. Phys. Plasmas Fluids Relat. Interdiscip. Top.*, vol. 81, no. 2, Feb. 2010, Art. no. 021124.
[22] Q. He and J. Wang, "Effects of multiscale noise tuning on stochastic resonance for weak signal detection," *Digit. Signal Process.*, vol. 22, no. 4, pp. 614–621, Jul. 2012.
[23] W. Zhao, J. Wang, and L. Wang, "The unsaturated bistable stochastic resonance theory," *Chaos*, vol. 23, 2013, Art. no. 033117.
[24] Z. Qiao, Y. Lei, J. Lin, and F. Jia, "An adaptive unsaturated bistable stochastic resonance method and its application in mechanical fault diagnosis," *Mech. Syst. Signal Process.*, vol. 84, pp. 731–746, Feb. 2017.
[25] L. Wang and B. Xia, "Binary aperiodic stochastic resonance based on piecewise hybrid system," in *Proc. 30th Chin. Control Conf.*, vol. 84, 2011, pp. 717–720.
[26] Y.-F. Guo, Y.-J. Shen, B. Xi, and J.-G. Tan, "Colored correlated multiplicative and additive Gaussian colored noises-induced transition of a piecewise nonlinear bistable model," *Modern Phys. Lett. B*, vol. 31, no. 28, Oct. 2017, Art. no. 1750256.
[27] F. Duan, L. Duan, F. Chapeau-Blondeau, Y. Ren, and D. Abbott, "Binary signal transmission in nonlinear sensors: Stochastic resonance and human hand balance," *IEEE Instrum. Meas. Mag.*, vol. 23, no. 1, pp. 44–49, Feb. 2020.
[28] G. Hu, "Stochastic forces and nonlinear systems," Shanghai Sci. Technol. Museum, Shanghai, China, Tech. Rep., 1995.
[29] S. Wang and F. Wang, "Adaptive stochastic resonance system in terahertz radar signal detection," *Acta Phys. Sin.*, vol. 67, no. 16, 2018, Art. no. 160502.
[30] L. Duan, F. Duan, F. Chapeau-Blondeau, and D. Abbott, "Stochastic resonance in hopfield neural networks for transmitting binary signals," *Phys. Lett. A*, vol. 384, no. 6, Feb. 2020, Art. no. 126143.
[31] Z. Lai, "Weak-signal detection based on the chaotic and stochastic-resonance characteristic of duffing oscillator," Tianjin Univ., Tianjin, China, Tech. Rep., 2014.
[32] J. Casado-Pascual, J. Gómez-Ordóñez, and M. Morillo, "Stochastic resonance: Theory and numerics," *Chaos, Interdiscipl. J. Nonlinear Sci.*, vol. 15, no. 2, Jun. 2005, Art. no. 026115.
[33] Y. Gao and F. Wang, "Adaptive cascaded-bistable stochastic resonance system research and design," *J. Comput. Theor. Nanoscience*, vol. 10, no. 2, pp. 318–322, Feb. 2013.
[34] J. E. Mottershead, C. Mares, S. James, and M. I. Friswell, "Stochastic model updating: Part 2—Application to a set of physical structures," *Mech. Syst. Signal Process.*, vol. 20, no. 8, pp. 2171–2185, Nov. 2006.
[35] X. Xu, Z. Qiao, and Y. Lei, "Repetitive transient extraction for machinery fault diagnosis using multiscale fractional order entropy infogram," *Mech. Syst. Signal Process.*, vol. 103, pp. 312–326, Mar. 2018.
[36] J. Liu, Y. Leng, Z. Lai, and S. Fan, "Multi-frequency signal detection based on frequency exchange and re-scaling stochastic resonance and its application to weak fault diagnosis," *Sensors*, vol. 18, no. 5, p. 1325, 2018.
[37] T. Chen, S. Ju, X. Yuan, M. Elhoseny, F. Ren, M. Fan, and Z. Chen, "Emotion recognition using empirical mode decomposition and approximation entropy," *Comput. Electr. Eng.*, vol. 72, pp. 383–392, Nov. 2018.
[38] J. Zhou, J. Ma, H. Xu, and X. Huang, "Application of EMD denoising method in subgrade settlement prediction of high-speed railways," *J. Vib. Shock*, vol. 35, pp. 66–72, 2016.
[39] J. Antoni, "The infogram: Entropic evidence of the signature of repetitive transients," *Mech. Syst. Signal Process.*, vol. 74, pp. 73–94, Jun. 2016.
[40] D. Ho and R. B. Randall, "Optimisation of bearing diagnostic techniques using simulated and actual bearing fault signals," *Mech. Syst. Signal Process.*, vol. 14, no. 5, pp. 763–788, Sep. 2000.
[41] G. Qin, D. Gong, G. Hu, and X. Wen, "An analog simulation of stochastic resonance," *Acta Phys. Sin.*, vol. 41, pp. 360–369, 1992.
[42] S. Sun, *Weak Signal Detection and Estimation*. Beijing, China: Electronic Industry Press, 2013.

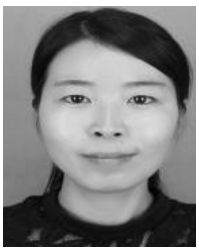

SHAN WANG is currently pursuing the Ph.D. degree with the School of Mechanical Engineering, Tiangong University, China. Her research interests include intelligent signal processing, fault bearing diagnosis, terahertz radar detection, and image enhancement.

PINGJUAN NIU received the Ph.D. degree from the School of Microelectronics, Tianjin University, in 2002. She is a Professor with the School of Electronics and Information Engineering, Tiangong University. Her research interests include intelligent signal processing, intelligent sensor and system integration, and bearing fault diagnosis.

YONGFENG GUO received the Ph.D. degree from the School of Science, Northwestern Polytechnic University, in 2010. He is a Professor with the School of Mathematical Sciences, Tiangong University. His research interests include the application of probability statistics, stochastic dynamical systems, and information theory.

FUZHONG WANG received the Ph.D. degree from the Beijing University of Science and Technology. He is a Professor with the School of Physical Science and Technology, Tiangong University. His research interests include stochastic resonance, noise processing, and signal amplification.

SHUZHEN HAN is currently pursuing the Ph.D. degree with the School of Mechanical Engineering, Tiangong University, China. Her research interests include image processing, bearing fault diagnosis, and intelligent measurement techniques.